


Wrinkling of liquid-crystal elastomer disks caused by light-driven dynamic contractionJun Zhao , Yong Yu, Peibao Xu, and Kai Li ^{*}*Department of Civil Engineering, Anhui Jianzhu University, Hefei, Anhui Province 230601, People's Republic of China*

(Received 23 December 2020; revised 21 February 2021; accepted 24 March 2021; published 21 April 2021)

The trigger time of light-driven wrinkling is very critical for accurate active control in photo-powered machines. In this paper, the wrinkling of liquid-crystal elastomer disks caused by light-driven dynamic contraction is theoretically studied, and the critical times for appearance and disappearance of the wrinkles are numerically calculated. The light-driven prebuckling stress can be significantly adjusted by changing the contraction coefficient, while controlled within a certain limit by tuning the light intensity and illumination time. There exists a critical contraction coefficient for triggering the wrinkling of the disk, and the second-order mode of wrinkling is the most unstable mode, which is most easily induced for the illumination radius ratio 0.69. The critical times for the appearance and disappearance of wrinkling can be significantly changed by the contraction coefficient, while regulated only within a certain range by the light intensity and the illumination radius ratio. These results have potential applications for accurate active control in the fields of soft robotics, active microlens, smart windows, and tunable surface patterns.

DOI: [10.1103/PhysRevE.103.L041002](https://doi.org/10.1103/PhysRevE.103.L041002)**I. INTRODUCTION**

Liquid-crystal elastomers (LCEs) are synthesized by anisotropic rodlike liquid-crystal molecules and the stretchable long-chain polymers, which have unique characteristics including big actuation stress of 300 kPa [1] and big actuation strain of 400% [2]. Nematic elastomers are the widespread thermotropic elastomers, which shrink along and stretch perpendicular to the nematic director in respond to heat [3], electric field [4], light [5,6], magnetic field [7], and chemicals [8], etc. This large, anisotropic, spontaneous, and reversible deformation has been widely used in the fields of artificial muscles [9,10], motors [11,12], soft actuators and sensors [13–15], tunable optical and tactile devices [16], and stretchable optical devices [17].

Light is widespread and easily available in nature. Furthermore, light has many unique advantages, which make it have great application value. For example, its characteristic parameters such as wavelength, intensity, and polarization provide broad design space for practical application requirements, and can realize the precise control of light in the equipment [18]. In recent years, more and more attention has been paid to the light-driven deformation of LCE. Yu *et al.* experimentally realized the reversible photoinduced bending of azobenzene chromophore for the first time [19]. By designing defects and structures reasonably, the photoinduced patterns can be accurately controlled [20,21]. Recently, a variety of light-powered robots which can “walk” [22–24] and “swim” [25,26] have been realized by using LCE materials. In addition, many scholars have established theoretical models to describe the photo-driven bending of LCE beams [27,28] and LCE plates [29–31].

Recently, light-driven morphological wrinkles of LCEs have attracted many scholars' attention [32–38]. It is very important to understand the wrinkling of LCEs, for it can be used to design and manufacture new devices [11], and sometimes should be inhibited for the stability of the structures [21]. Yang and He analytically obtained the critical buckling load and buckling mode of glassy nematic films [32], and numerically achieved the accurate wrinkling patterns [33]. Fu *et al.* theoretically and numerically investigated the appearance and evolution of wrinkling patterns of LCE films under various distributed light illumination [34]. Agrawal *et al.* fabricated a bilayer made of LCEs and polystyrene, and the bilayer can reversibly buckle into regular patterns [35,36]. Sun *et al.* used light as a viable controlling approach to buckle thin films and obtain various spatial morphologies of buckling [37].

In the above-mentioned works on light-induced wrinkling, it is assumed that the light-driven deformation is time independent. In fact, the light-driven deformation is always time dependent. Recently, the light-driven dynamic deformation has attracted extensive attention [27,29,38]. To our knowledge, how the light-driven dynamic contraction affects wrinkling of LCE has rarely been investigated, which has potential applications for accurate active control in the fields of soft robotics, active microlens, smart windows, and tunable surface patterns. In this paper, we theoretically explore the wrinkling of LCE disks caused by light-driven dynamic contraction, and calculate the critical times for appearance and disappearance of wrinkling. First, we combine the nonlinear von Kármán plate theory and dynamic LCE model to establish an LCE plate model. Then, we calculate the prebuckling stress distribution and several wrinkling modes of the LCE disk under a certain illumination radius ratio. Finally, we conduct linear stability analysis to obtain the critical material contraction coefficient for the wrinkling and the critical times for the appearance and disappearance of wrinkling.

^{*}kli@ahjzu.edu.cn

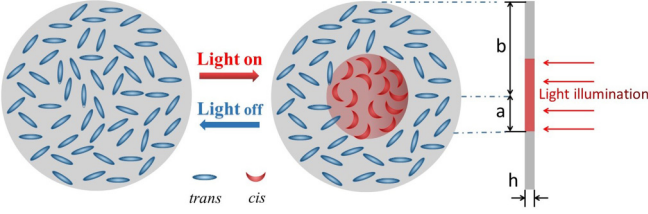


FIG. 1. Schematic model of a thin, freestanding LCE disk, with radius b and the thickness h . The disk is homogeneously illuminated vertically by light in a circular core area of radius a . The azobenzene liquid-crystal molecules are planar anchored and randomly distributed in the thin LCE disk.

II. DYNAMIC OF PHOTOELASTOMERS

Figure 1 sketches a thin, freestanding LCE disk with radius b , which is homogeneously illuminated vertically in a circular core area of radius a . According to Yu *et al.*, the UV light with wavelength less than 400 nm or laser can induce *trans*-to-*cis*-isomerization [19]. Under the UV light excitation, light-driven *cis*-to-*trans*-isomerization can be neglected [39,40]. Therefore, the number fraction of *cis*-isomers $\phi(z, t)$ depends on thermal excitation from *trans*- to *cis*-, thermally driven relaxation from *cis*- to *trans*-, and light-driven *trans*-to-*cis*-isomerization. Considering that thermal excitation from *trans*- to *cis*- is often negligible relative to the light-driven excitation [41,42], evolution of $\phi(z, t)$ can be usually described by the governing equation [41,42]

$$\frac{\partial \phi}{\partial t} = \eta_0 I (1 - \phi) - T_0^{-1} \phi, \quad (1)$$

where T_0 is the thermal relaxation time from the *cis*- to *trans*-state and η_0 is a light-absorption constant. In general, the ratio between the *cis*-to-*trans*- and *trans*-to-*cis*-absorption coefficients defines the light penetration depth [39,40]. For simplicity, we assume the thickness is much smaller than the penetration depth, and the light intensity I decays slightly with the depth of the disk [32]. Therefore, $\phi(z, t)$ is independent of z , i.e., $\phi(z, t) = \phi(t)$.

We assume that the azobenzene liquid-crystal molecules are planar anchored and randomly distributed in the LCE disk. Although it is very challenging to fabricate this sample for the experiment, one could create a thin polydomain film with small, randomly oriented nematic domains by using a photoalignment technique actually [43]. When under the UV-light excitation, the irradiated area contracts uniformly in the plane and expands in the direction of thickness. For simplicity, we assume that the fraction of azobenzene is far less than 1. Therefore, by carrying out Taylor expansion and keeping only the linear order term, the light-driven contraction strain $\varepsilon_0(t)$ is proportional to the small *cis*-isomer number fraction $\phi(t)$, i.e., $\varepsilon_0(t) = -C_0 \phi(t)$, with C_0 being the phenomenological contraction coefficient and relating the light-driven contraction with *cis*-isomer number fraction. The solution to Eq. (1) can be easily obtained, and the light-driven contraction strain

is calculated as

$$\varepsilon_0(\bar{t}) = -\frac{C_0 \bar{I}}{\bar{I} + 1} - C_0 \left(\phi_0 - \frac{\bar{I}}{\bar{I} + 1} \right) \exp[-\bar{t}(\bar{I} + 1)], \quad (2)$$

where $\bar{I} = \eta_0 T_0 I$, $\bar{t} = t/T_0$, and ϕ_0 is the *cis*-number fraction of the photochromic molecules at $t = 0$. It can be seen from Eq. (2), for given C_0 , with the increase of light intensity or illumination time, the light-driven strain has upper limit. Conversely, for given light intensity and illumination time, with the increase of C_0 , the light-driven strain increases linearly, and there is no upper limit.

The radial and hoop stresses in the disk caused by the light-driven contraction strain can be easily given by Ref. [44].

$$\begin{aligned} \sigma_{rr}^{(0)} &= \frac{E \varepsilon_0}{2} \left[\lambda^2 - 1 - \left(\frac{\lambda^2}{\rho^2} - 1 \right) H(\rho - \lambda) \right], \\ \sigma_{\theta\theta}^{(0)} &= \frac{E \varepsilon_0}{2} \left[\lambda^2 - 1 + \left(\frac{\lambda^2}{\rho^2} + 1 \right) H(\rho - \lambda) \right], \end{aligned} \quad (3)$$

where $\rho = r/b$, $\lambda = a/b$, E is Young's modulus, and $H(\rho - \lambda)$ is the unit step function.

III. LINEAR STABILITY ANALYSIS

We represent out-of-plane deflection of the disk as $W = W(r, \theta)$. According to the von Kármán equation, the linearized bifurcation equation governing the wrinkling of the disk can be given as [45]

$$D \nabla^4 W - h \left[\sigma_{rr}^{(0)} \frac{\partial^2 W}{\partial r^2} + \sigma_{\theta\theta}^{(0)} \frac{1}{r} \left(\frac{\partial W}{\partial r} + \frac{1}{r} \frac{\partial^2 W}{\partial \theta^2} \right) \right] = 0, \quad (4)$$

where $D = Eh^3/12(1 - \nu^2)$ is the bending stiffness, ν is the Poisson ratio, and h is the thickness of the disk. Here, $\nabla^2 = \partial^2/\partial r^2 + \partial/r\partial r + \partial^2/r^2\partial\theta^2$ is the Laplacian operator in polar coordinates, and $\nabla^4(\bullet) \equiv \nabla^2(\nabla^2(\bullet))$. For the purpose of eliminating the purely rigid-body displacement of the disk, the center of the disk is taken to be fixed, and the outer edge is stress free. The associated boundary conditions are given as $r^2 \partial^2 w/\partial r^2 + \nu(r \partial w/\partial r + \partial^2 w/\partial \theta^2) = 0$, $r \partial(\nabla^2 w)/\partial r + (1 - \nu) \partial^2(\partial w/r\partial \theta)/\partial r \partial \theta = 0$ at $r = b$, and $w = 0$, $\partial w/\partial r = 0$ at $r = 0$ [45].

To solve the bifurcation equation (4), we set $W = f(\rho) \cos(n\theta)$, where $n \in \mathbb{N}$ is the wave number (the number of identical circumferential wrinkles) and $f(\rho)$ satisfies the following differential equation:

$$\begin{aligned} \frac{d^4 f}{d\rho^4} + \frac{2}{\rho} \frac{d^3 f}{d\rho^3} - \left(\frac{2n^2 + 1}{\rho^2} + \frac{hb^2 \sigma_{rr}^{(0)}}{D} \right) \frac{d^2 f}{d\rho^2} \\ + \frac{1}{\rho} \left(\frac{2n^2 + 1}{\rho^2} - \frac{hb^2 \sigma_{\theta\theta}^{(0)}}{D} \right) \frac{df}{d\rho} \\ + \frac{n^2}{\rho^2} \left(\frac{n^2 - 4}{\rho^2} + \frac{hb^2 \sigma_{\theta\theta}^{(0)}}{D} \right) f = 0. \end{aligned} \quad (5)$$

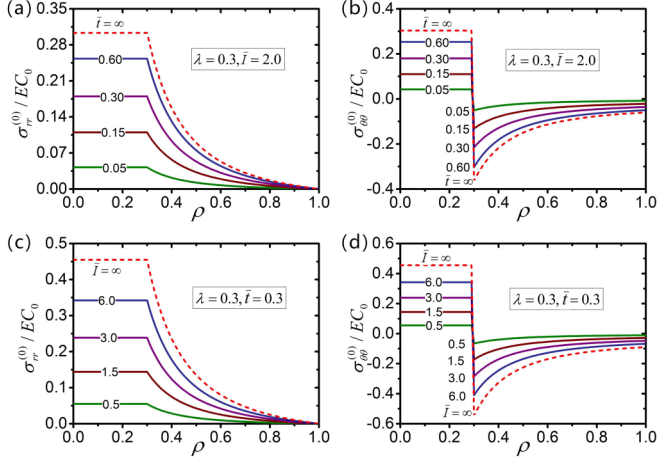


FIG. 2. The dimensionless prebuckling radial (a), (c) and hoop stress (b), (d) distributions of the LCE disk under illumination radius ratio $\lambda = 0.3$ for different light intensities \bar{I} and illumination times \bar{t} . It is noted that the prebuckling stresses are linear to the contraction coefficient C_0 .

The corresponding boundary conditions for $f(\rho)$ can also be derived as

$$\begin{aligned}
 f|_{\rho=0} &= 0, \\
 \frac{df}{d\rho}\Big|_{\rho=0} &= 0, \\
 \rho^2 \frac{d^2 f}{d\rho^2} + \nu \left(\rho \frac{df}{d\rho} - n^2 f \right) \Big|_{\rho=1} &= 0, \\
 \rho^3 \frac{d^3 f}{d\rho^3} + \rho^2 \frac{d^2 f}{d\rho^2} - \rho [1 + (2 - \nu)n^2] \frac{df}{d\rho} \\
 + (3 - \nu)n^2 f \Big|_{\rho=1} &= 0.
 \end{aligned} \tag{6}$$

Equation (5) associated with the corresponding boundary condition (6) gives the eigenvalue problem for the wrinkling of the LCE disk, which can be numerically solved by the module *bvp4c* in MATLAB software.

IV. PREBUCKLING STRESSED STATES DRIVEN BY ILLUMINATION

Based on Eq. (3), we can obtain the prebuckling stress distribution in the disk. In the following computation, we set $b/h = 100$ and $\nu = 0.5$ [46,47]. Figure 2 illustrates the radial and hoop stress distribution of the LCE disk under illumination radius ratio $\lambda = 0.3$ for different light intensity \bar{I} , illumination time \bar{t} , and the contraction coefficient C_0 . It is seen that the radial stress $\sigma_{rr}^{(0)}$ and hoop stress $\sigma_{\theta\theta}^{(0)}$ in the illumination zone are equal to a constant greater than zero, that is, the illumination zone is in tensile hydrostatic pressure state. Outside the illumination zone, with the increasing ρ , the tensile radial stress decreases continuously to zero at the boundary of the disk, while the compressive hoop stress is discontinuous at the boundary of the illumination zone, and decreases continuously, which is the cause of wrinkling.

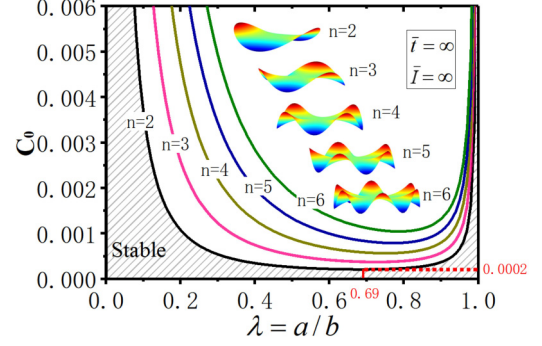


FIG. 3. Critical contraction coefficient C_0 for wrinkling instabilities of different modes in the LCE disk under different illumination radius ratios $\lambda = a/b$, in the case of infinite light intensity and infinite illumination time. In the computation, $\nu = 0.5$ and $b/h = 100$.

It is noted that the prebuckling stress is linear to the contraction coefficient C_0 , which can be seen from Eq. (3). Figures 2(a) and 2(b) show that for given light intensity ($\bar{I} = 2$), with the increase of illumination time, the stress amplitude increases nonlinearly and finally approaches an asymptotic state shown by the red line, which is easily understood from Eqs. (2) and (3). Figures 2(c) and 2(d) show that for given illumination time ($\bar{t} = 0.3$), with the increase of the light intensity, the stress amplitude increases nonlinearly and also finally approaches an asymptotic state shown by the red line. It can be seen that the prebuckling stress can be significantly adjusted by changing the contraction coefficient, while regulated within a certain limit by tuning the light intensity and illumination time.

V. WRINKLING BEHAVIORS

As shown in Eq. (2) and Fig. 2, the light-driven strain approaches the maximum value C_0 , in the case of infinite light intensity and infinite illumination time. Herein, Fig. 3 shows the critical contraction coefficient C_0 for wrinkling instabilities of different modes in the LCE disk under different illumination radius ratios $\lambda = a/b$, in cases of infinite light intensity and infinite illumination time. It can be seen that, when the light shines on the central zone of the LCE disk, it can induce the wrinkling mode $n \geq 2$. This is because the region outside the illumination zone wrinkles out of the surface to release the hoop compressive stress. For a given illumination radius ratio $\lambda = a/b$, with increasing wrinkling mode n , the critical contraction coefficient C_0 increases. Therefore, the second-order wrinkling mode is most easily to occur.

For a given wrinkling mode n , the critical contraction coefficient C_0 first decreases and then increases with the increase of the radius ratio λ . There is a minimum critical contraction coefficient for the second-order wrinkling mode, which is $C_0 = 0.0002$ at $\lambda = 0.69$. There is a stable region in the disk that will not buckle, as shown by the shaded area in Fig. 3. The result means that the material contraction coefficient must be greater than a critical value for triggering the wrinkling of the disk. This result can guide the selection of materials in practical applications.

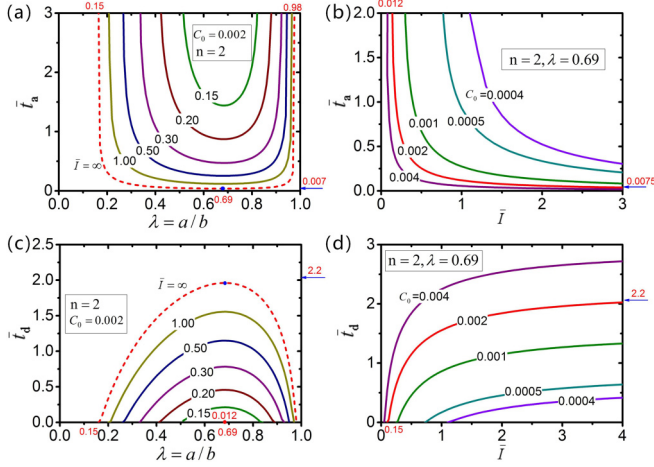


FIG. 4. The critical times for the appearance and disappearance of wrinkling of second-order mode under different illumination radius ratios and light intensities.

VI. DYNAMIC EFFECTS

Next, we discuss the appearance critical time \bar{t}_a and the disappearance critical time \bar{t}_d of wrinkling, in which \bar{t}_a is the required time for the disk from light on to wrinkling, and \bar{t}_d is the required time from light off to wrinkle disappear. In the calculation, we assumed that the increasing buckling deformation of the disk does not influence the illumination zone. Figure 4(a) shows the variation of the critical time \bar{t}_a of the second-order wrinkling mode with the illumination radius ratio λ for $C_0 = 0.002$. With the increase of λ , \bar{t}_a first decreases and then increases. When the illumination radius ratio $\lambda = 0.69$, \bar{t}_a is minimum. Under a given light intensity, there is an instability region of illumination radius ratio, and outside this region \bar{t}_a is infinite, that is, wrinkling does not occur. With the increase of light intensity, this region increases. It is noted that when $\bar{I} \rightarrow \infty$, the region has a limit range $0.15 \leq \lambda \leq 0.98$.

Furthermore, given the illumination radius ratio $\lambda = 0.69$, \bar{t}_a increases with decreasing \bar{I} . When $\bar{I} \leq 0.012$, \bar{t}_a approaches infinity, that is, no wrinkling occurs. This can be understood from Eq. (2) that for given C_0 , when light intensity or illumination time approaches infinity, the light-driven strain has upper limit [38]. The result implies that there exists a minimum light intensity for triggering the wrinkling. Meanwhile, \bar{t}_a decreases with the increasing \bar{I} , and there is a minimum critical time $\bar{t}_a = 0.0075$, as shown in Figs. 4(a) and 4(b). Additionally, Fig. 4(b) shows that for a given light intensity, the larger the material contraction coefficient C_0 is, the smaller the critical time \bar{t}_a is.

Figure 4(c) shows the change of the critical time \bar{t}_d of the second-order wrinkling mode with the illumination radius ratio λ for $C_0 = 0.002$. With the increase of λ , \bar{t}_d first increases and then decreases. Given the illumination radius ratio $\lambda = 0.69$, \bar{t}_d increases with increasing \bar{I} , and approaches

an upper limit value $\bar{t}_d = 2.2$. Meanwhile, when $\bar{I} \leq 0.012$, $\bar{t}_d = 0$, that is, no wrinkling occurs, as shown in Figs. 4(c) and 4(d). Additionally, Fig. 4(d) shows that for a given light intensity, the larger the material contraction coefficient C_0 is, the larger the critical time \bar{t}_d is. It is concluded that the critical times \bar{t}_a and \bar{t}_d can be significantly controlled by the contraction coefficient, while can be regulated only within a certain range by the light intensity and the illumination radius ratio.

The LCE plate model adopted in this paper ignores the slight curvature of the disk due to the inhomogeneous contraction caused by attenuating light intensity along the thickness, which may slightly affect the quantitative analysis results, while the qualitative analysis results should be reliable. Moreover, the model and analytical method proposed in this paper are universal and have value for analyzing wrinkling of LCE plates caused by illumination with arbitrary spatial and time-resolved distribution. We hope that the results in this paper can benefit for deepening the understanding of the buckling caused by light-driven dynamic contraction, so as to guide the subsequent experiments and engineering applications.

VII. CONCLUSION AND DISCUSSION

The wrinkling of LCE disk can be caused by light-driven dynamic contraction. Through linear stability analysis, we numerically calculate the critical contraction coefficient, the critical times for appearance and disappearance of the wrinkles. The prebuckling stress can be significantly adjusted by changing the contraction coefficient, while changed within a certain limit by changing the light intensity and illumination time. There exists a critical contraction coefficient for triggering the wrinkling of the disk, and the second-order mode of wrinkling is the most unstable mode, which is most easily induced for the illumination radius ratio 0.69. The results show that the critical times for the appearance and disappearance of wrinkling depend on the illumination radius ratio, light intensity, and material contraction coefficient, which can be significantly controlled by the contraction coefficient, while regulated only within a certain range by the light intensity and the illumination radius ratio. In practice, the phenomenological contraction coefficient can be experimentally controlled by the ways of adjusting the fraction of photochromic molecules, etc., for achieving accurate active control in the fields of soft robotics, active microlens, smart windows, and tunable surface patterns.

ACKNOWLEDGMENTS

The authors acknowledge the financial support from University Natural Science Research Project of Anhui Province (Grants No. KJ2019A0740, No. KJ2020A0449, and No. KJ2020A0452), and Doctoral Startup Foundation from Anhui Jianzhu University (Grant No. 2018QD09).

- [1] J. Naciri, A. Srinivasan, H. Jeon, N. Nikolov, P. Keller, and B. R. Ratna, Nematic elastomer fiber actuator, *Macromolecules* **36**, 8499 (2003).
- [2] H. Yang, A. Buguin, J. M. Taulemesse, K. Kaneko, S. Méry, A. Bergeret, and P. Keller, Micron-sized main-chain liquid crystalline elastomer actuators with ultralarge amplitude contractions, *J. Am. Chem. Soc.* **131**, 15000 (2009).
- [3] T. H. Ware, M. E. McConney, J. J. Wie, V. P. Tondiglia, and T. J. White, Voxelated liquid crystal elastomers, *Science* **347**, 982 (2015).
- [4] Y. H. Na, Y. Aburaya, H. Orihara, and K. Hiraoka, Measurement of electrically induced shear strain in a chiral smectic liquid-crystal elastomer, *Phys. Rev. E* **83**, 061709 (2011).
- [5] H. Zeng, O. M. Wani, P. Wasylczyk, R. Kaczmarek, and A. Priimagi, Self-regulating iris based on light-actuated liquid crystal elastomer, *Adv. Mater.* **29**, 1701814 (2017).
- [6] K. Kumar, C. Knie, D. Bléger, M. A. Peletier, H. Friedrich, S. Hecht, D. J. Broer, M. G. Debije, and A. P. H. J. Schenning, A chaotic self-oscillating sunlight-driven polymer actuator, *Nat. Commun.* **7**, 11975 (2016).
- [7] J. M. Haberl, A. Sanchez-Ferrer, A. M. Mihut, H. Dietsch, A. M. Hirt, and R. Mezzenga, Liquid-crystalline elastomer-nanoparticle hybrids with reversible switch of magnetic memory, *Adv. Mater.* **25**, 1787 (2013).
- [8] K. D. Harris, C. W. Bastiaansen, J. Lub, and D. J. Broer, Self-assembled polymer films for controlled agent-driven motion, *Nano Lett.* **5**, 1857(2005).
- [9] M. H. Li and P. Keller, Artificial muscles based on liquid crystal elastomers, *Philos. Trans. Roy. Soc. A* **364**, 2763 (2006).
- [10] P. G. De Gennes, A semi-fast artificial muscle, *C. R. Acad. Sci. Paris, Ser. IIB* **324**, 343 (1997).
- [11] M. Camacho-Lopez, H. Finkelmann, P. Palfy-Muhoray, and M. Shelley, Fast liquid-crystal elastomer swims into the dark, *Nat. Mater.* **3**, 307 (2004).
- [12] M. Yamada, M. Kondo, J. I. Mamiya, Y. Yu, M. Kinoshita, C. J. Barrett, and T. Ikeda, Photomobile polymer materials: Towards light-driven plastic motors, *Angew. Chem. Int. Ed.* **47**, 4986 (2008).
- [13] P. Palfy-Muhoray, Liquid crystals: Printed actuators in a flap, *Nat. Mater.* **8**, 614 (2009).
- [14] C. L. van Oosten, C. W. M. Bastiaansen, and D. J. Broer, Printed artificial cilia from liquid-crystal network actuators modularly driven by light, *Nat. Mater.* **8**, 677(2009).
- [15] H. Finkelmann, E. Nishikawa, and Pereira, and M. Warner, A New Opto-Mechanical Effect in Solids, *Phys. Rev. Lett.* **87**, 015501 (2001).
- [16] N. Torras, K. E. Zinoviev, C. J. Camargo, E. M. Campo, H. Campanella, J. Esteve, J. E. Marshall, E. M. Terentjev, M. Omastova, I. Krupa, P. Teplicky, B. Mamojka, P. Bruns, B. Roeder, M. Vallribera, R. Malet, S. Zuffanelli, V. Soler, J. Roig, N. Walker *et al.*, Tactile device based on opto-mechanical actuation of liquid crystal elastomers, *Sens. Actuators Phys.* **208**, 104 (2014).
- [17] N. J. Dawson, M. G. Kuzyk, J. Neal, P. Luchette, and P. Palfy-Muhoray, Cascading of liquid crystal elastomer photomechanical optical devices, *Opt. Commun.* **284**, 991 (2011).
- [18] H. Zeng, P. Wasylczyk, D. S. Wiersma, and A. Priimagi, Light robots: Bridging the gap between microrobotics and photomechanics in soft materials, *Adv. Mater.* **30**, 1703554 (2017).
- [19] Y. Yu, M. Nakano, and T. Ikeda, Photomechanics: Directed bending of a polymer film by light-miniaturizing a simple photomechanical system could expand its range of applications, *Nature (London)* **425**, 145 (2003).
- [20] S. K. Ahn, T. H. Ware, K. M. Lee, V. P. Tondiglia, and T. J. White, Photoinduced topographical feature development in blueprinted azobenzene functionalized liquid crystalline elastomers, *Adv. Funct. Mater.* **26**, 5819 (2016).
- [21] K. Fuchi, T. H. Ware, P. R. Buskohl, G. W. Reich, R. A. Vaia, T. J. White, and J. J. Joo, Topology optimization for the design of folding liquid crystal elastomer actuators, *Soft Matter* **11**, 7288 (2015).
- [22] M. Rogó, H. Zeng, C. Xuan, D. S. Wiersma, and P. Wasylczyk, Light-driven soft robot mimics caterpillar locomotion in natural scale, *Adv. Opt. Mater.* **4**, 1689 (2016).
- [23] A. H. Gelebart, D. J. Mulder, M. Varga, A. Konya, G. Vantomme, E. W. Meijer, R. L. B. Selinger, and D. J. Broer, Making waves in a photoactive polymer film, *Nature (London)* **546**, 632(2017).
- [24] H. Zeng, O. M. Wani, P. Wasylczyk, and A. Priimagi, Light-driven caterpillar inspired miniature inching robot, *Macromol. Rapid Commun.* **39**, 1700224 (2017).
- [25] C. Huang, J. A. Lv, X. Tian, Y. Wang, and Y. Yu, and J. Liu, Miniaturized swimming soft robot with complex movement actuated and controlled by remote light signals, *Sci. Rep.* **5**, 17414 (2015).
- [26] S. Palagi, A. G. Mark, S. Y. Reigh, K. Melde, T. Qiu, H. Zeng, C. Parmeggiani, D. Martella, A. Sanchez-Castillo, N. Kapernaum, F. Giesselmann, D. S. Wiersma, and E. Lauga, and P. Fischer, Structured light enables biomimetic swimming and versatile locomotion of photoresponsive soft microrobots, *Nat. Mater.* **15**, 647 (2016).
- [27] D. Zhao and Y. Liu, Photomechanical vibration energy harvesting based on liquid crystal elastomer cantilever, *Smart Mater. Struct.* **28**, 075017 (2019).
- [28] L. Jin, Y. Lin, and Y. Huo, A large deflection light-induced bending model for liquid crystal elastomers under uniform or non-uniform illumination, *Int. J. Solids Struct.* **48**, 3232 (2011).
- [29] A. M. Parrany, Nonlinear light-induced vibration behavior of liquid crystal elastomer beam, *Int. J. Mech. Sci.* **136**, 179 (2018).
- [30] M. L. Dunn and K. Maute, Photomechanics of blanket and patterned liquid crystal elastomer films, *Mech. Mater.* **41**, 1083 (2009).
- [31] C. Fu, Y. Xu, F. Xu, and Y. Huo, Light-induced bending and buckling of large deflected liquid crystalline polymer plates, *Int. J. Appl. Mech.* **08**, 1640007 (2016).
- [32] D. Yang and L. H. He, Photo-triggered wrinkling of glassy nematic films, *Smart Mater. Struct.* **23**, 045012 (2014).
- [33] D. Yang and L. H. He, Nonlinear analysis of photo-induced wrinkling of glassy twist nematic films on compliant substrates, *Acta Mech. Sin.* **31**, 672 (2015).
- [34] C. Fu, F. Xu, and Y. Huo, Photo-controlled patterned wrinkling of liquid crystalline polymer films on compliant substrates, *Int. J. Solids Struct.* **132-133**, 264 (2018).
- [35] A. Agrawal, P. Luchette, P. Palfy-Muhoray, S. L. Biswal, W. G. Chapman, and R. Verduzco, Surface wrinkling in liquid crystal elastomers, *Soft Matter* **8**, 7138 (2012).

- [36] A. Agrawal, T. Yun, and S. L. Pesek, W. G. Chapman, and R. Verduzco, Shape-responsive liquid crystal elastomer bilayers, *Soft Matter* **10**, 1411 (2014).
- [37] J. Y. Sun, S. Xia, M. W. Moon, K. H. Oh, and K. S. Kim, Folding wrinkles of a thin stiff layer on a soft substrate, *Proc. R. Soc. A* **468**, 932 (2012).
- [38] J. Zhao, P. Xu, Y. Yu, and K. Li, Controllable vibration of liquid crystal elastomer beams under periodic illumination, *Int. J. Mech. Sci.* **170**, 105366 (2020).
- [39] M. Gregorc, B. Zalar, V. Domenici, G. Ambrožič, I. Drevenšek-Olenik, M. Fally, and M. Čopič, Depth profile of optically recorded patterns in light-sensitive liquid-crystal elastomers, *Phys. Rev. E* **84**, 031707 (2011).
- [40] S. Waitukaitis, P. Dieleman, and M. van Hecke, Non-Euclidean origami, *Phys. Rev. E* **102**, 031001(R) (2020).
- [41] T. Nagele, R. Hoche, W. Zinth, and J. Wachtveitl, Femtosecond photoisomerization of cis-azobenzene, *Chem. Phys. Lett.* **272**, 489 (1997).
- [42] M. Warner and E. M. Terentjev, *Liquid Crystal Elastomers* (Oxford University Press, Oxford, 2007).
- [43] V. G. Chigrinov, V. M. Kozenkov, and H. S. Kwok, *Photoalignment of Liquid Crystalline Materials: Physics and Applications* (John Wiley & Sons, Chichester, England, 2008).
- [44] K. Li, S. P. Yan, Y. Ni, H. Y. Liang, and L. H. He, Controllable buckling of an elastic disc with actuation strain, *EPL* **92**, 16003 (2010).
- [45] E. Ventsel and T. Krauthammer, *Thin Plates and Shells: Theory, Analysis, and Applications* (Marcel Dekker, New York, 2001), Chap. 4.
- [46] W. T. Ren, P. J. McMullan, and A. C. Griffin, Poisson's ratio of monodomain liquid crystalline elastomers, *Macromol. Chem. Phys.* **209**, 1896(2008).
- [47] V. Aksenov, J. Blasing, R. Stannarius, M. Rossle, and R. Zentel, Strain-induced compression of smectic layers in free-standing liquid crystalline elastomer films, *Liq. Cryst.* **32**, 805 (2005).